$Co^{2+/3+}$ and $Fe^{2+/3+}$ charge transition levels in (La,Sr)$CoO_{3-\delta}$ and (La, Sr)$FeO_{3-\delta}$

Yue Liu, Stefanie Frick, Katharina N. S. Lohaus, and Andreas Klein*
Institute of Materials Science, Electronic Structure of Materials, Technical University of Darmstadt, 64287 Darmstadt, Germany

(Received 22 January 2025; revised 25 April 2025; accepted 15 July 2025; published 25 July 2025)

X-ray photoelectron spectroscopy (XPS) is used to determine the energy levels associated with the $Co^{2+/3+}$ and $Fe^{2+/3+}$ charge transition levels in (La, Sr)$CoO_{3-\delta}$ and (La, Sr)$FeO_{3-\delta}$, respectively. The charge transition levels are revealed by varying the Fermi level by means of oxidizing and reducing treatments. The $Co^{2+/3+}$ transition occurs at 0.15 ± 0.05 eV above the valence band maximum of (La, Sr)$CoO_{3-\delta}$ and the $Fe^{2+/3+}$ transition at 1.25 ± 0.05 eV above the valence band maximum of (La, Sr)$FeO_{3-\delta}$, respectively. In combination with the energy band alignment determined from XPS analysis in the course of interface formation, it is derived that the energetic difference of the charge transition levels coincides with that in Co-doped $BiFeO_3$, suggesting transferability of the energy levels in perovskite-type materials. The difference in charge transition levels directly relates to the easier reduction of Co compared to Fe. The result emphasizes that the oxidation states of Fe and Co in mixed compounds must be treated independently for a quantitative description of (defect) properties. They also provide a natural direct explanation for the higher electronic conductivity of (La, Sr)$CoO_{3-\delta}$ compared to that of (La, Sr)$FeO_{3-\delta}$, and for the acceptor behavior of Co in (La, Sr)$FeO_{3-\delta}$.

DOI: 10.1103/tn7z-thjk

I. INTRODUCTION

Perovskite-type oxides with ABO_3 composition exhibit a wide range of properties. Their behavior can vary significantly based on composition and doping, displaying metallic, semiconducting, oxygen-ion conductive, proton conductive, or insulating characteristics [1]. Sr-doped transition metal lanthanides, LaMO_3 (M = Fe, Co), are known to be mixed ionic-electronic conductors, which are applied as electrode materials in solid oxide electrochemical cells or oxygen separation membranes [2–4]. Undoped stoichiometric materials are insulators at room temperature (RT) with energy gaps of 2.1 eV [5,6] for $LaFeO_3$ and <1 eV for $LaCoO_3$ [7–9].

The partial substitution of La by Sr corresponds to an acceptor doping and introduces negative charges, Sr'_{La}, on the A-site. To maintain charge neutrality, acceptor doping can be compensated by electron holes $h^\bullet$, oxygen vacancies $v_O^{\bullet\bullet}$, oxidation of the transition metal $M_M^\times \rightarrow M_M^\bullet$, or of the oxygen ion $O_O^\times \rightarrow O_O^\bullet$. For very high oxygen vacancy concentrations, a reduction of the transition metal may also occur, $M_M^\times \rightarrow M'_M$. The different compensation mechanisms can be categorized as electronic compensation, ionic compensation, and valence changes, respectively. Considering all potential charge compensation mechanisms, the charge neutrality for (La,Sr)$MO_{3-\delta}$ can be written with [...] denoting the defect concentrations per volume

$$[Sr'_{La}] + [M'_M] = [h^\bullet] + 2[v_O^{\bullet\bullet}] + [M_M^\bullet] + [O_O^\bullet]. \quad (1)$$

If all singly charged Sr acceptors are compensated by doubly charged oxygen vacancies, i.e., if $[M'_M] = [h^\bullet] = [M_M^\bullet] = [O_O^\bullet] = 0$, the resulting oxygen vacancy concentration, $[v_O^{\bullet\bullet}]$, which equals the off-stoichiometry δ, corresponds to exactly half of the Sr concentration. As deduced from the charge neutrality equation, an increase of the oxygen vacancy concentration results in a decrease in the concentration of holes $h^\bullet$, oxidized transition metals $M_M^\bullet$, and oxidized oxygen $O_O^\bullet$. Conversely, a reduction of the transition metal M'_M becomes more favorable with an increasing oxygen vacancy concentration.

The defect chemistry of (La, Sr)$CoO_{3-\delta}$ (LSC) and (La, Sr)$FeO_{3-\delta}$ (LSF) is extensively described in the literature [10–12]. Although the same defects arise for LSC and LSF upon Sr doping, the electronic conductivity of LSC is significantly higher than that of LSF [13]. The difference must be related to a different preference of the competing charge compensation mechanisms. It was recently outlined that the Fermi level can be used as a common parameter for comparing the different compensation mechanisms [14]. This is possible as the concentration of every defect involved in Eq. (1) can be described by its Gibbs energy of formation ΔG_d, which exhibits a defined dependence on the Fermi level as illustrated in Fig. 1. The defect concentrations obtained by finding the equilibrium Fermi level are equivalent to those obtained from defect chemistry, where defects concentrations are derived from mass action laws of defect reactions and not from formation energies of individual defects [14–16]. The dependence of the defect concentrations on oxygen partial pressure, as described by defect chemistry, is included in Fig. 1 by the dependence of the Gibbs energies of formation of the ionic defects on the oxygen chemical potential [17].

An advantage of describing defect properties by the dependence of the Gibbs energies of defect formation on the Fermi level, as illustrated in Fig. 1, is that the Fermi level

*Contact author: aklein@esm.tu-darmstadt.de

Published by the American Physical Society under the terms of the Creative Commons Attribution 4.0 International license. Further distribution of this work must maintain attribution to the author(s) and the published article's title, journal citation, and DOI.

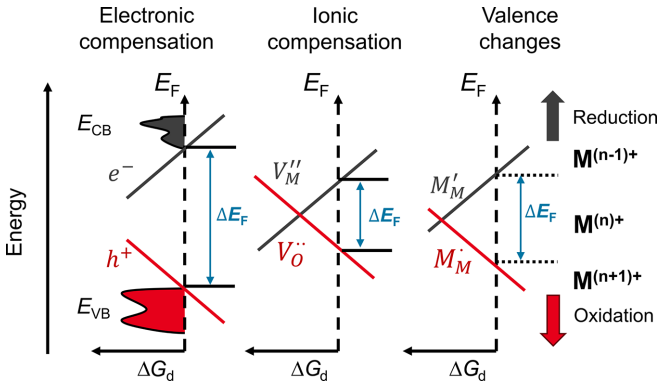


FIG. 1. Gibbs energies of formation of electronic and ionic defects and of cationic valence changes in a simple binary metal oxide exhibiting Schottky disorder with metal and oxygen vacancies as dominating ionic defects for a single value of the oxygen chemical potential. Only the formation enthalpies of the ionic defects depend on the oxygen chemical potential (oxygen partial pressure). The oxygen vacancy concentration can be varied by reducing or oxidizing treatments, resulting in an upward or downward shift of the Fermi level to higher or lower energies, respectively. Reducing treatments increases the concentration of oxygen vacancies and raises the Fermi level to higher energies. A reduction of the transition metal occurs when the Fermi level reaches the charge transition level at which the transition metal changes its oxidation state from $M^{(n)+}$ to $M^{(n-1)+}$. For oxidizing conditions, the oxygen vacancy concentration is reduced, resulting in a downward shift of the Fermi level and potentially to an oxidation of the transition metal or oxygen.

position can be directly determined using x-ray photoelectron spectroscopy (XPS) [18,19]. For oxides, the Fermi level at the surface of a sample can be varied by different reducing and oxidizing sample treatments. Combining such treatments with XPS analysis, the limits of the Fermi level induced by ionic compensation and/or by valence changes of the material's constituents can be identified. For example, it was demonstrated that the Fermi level in hematite Fe_2O_3 is limited to ≈0.5 eV below the conduction band minimum by the reduction of Fe, $Fe^{3+} \rightarrow Fe^{2+}$ [20]. By varying the Fermi level in Bi(Fe,Co)$O_{3-\delta}$, the $Fe^{2+/3+}$ and $Co^{2+/3+}$ charge transition levels were identified at 1.65 eV and 0.8 eV above the valence band maximum, respectively [21].

It would be highly beneficial for the design of materials if the charge transition levels could be transferred from one material to another. Such a transfer requires aligning the energy bands of materials on a suitable energy scale. A correlation between defect energy levels and band alignment was described first for transition metal impurities in semiconductors [22–24] and later also for hydrogen impurities [25] and oxygen vacancies [26]. The band alignment is also related to the catalytic activity at solid/gas and solid/electrolyte interfaces, where the charge transition levels of redox active species are important [27,28]. Aligning the energy bands of Fe_2O_3 and $BiFeO_3$ revealed, for example, that the $Fe^{2+/3+}$ charge transition occurs at the same energy in the two materials [21].

In this contribution the $Co^{2+/3+}$ and the $Fe^{2+/3+}$ charge transition levels in (La, Sr)$CoO_{3-\delta}$ and (La, Sr)$FeO_{3-\delta}$ are determined by means of XPS with a systematic variation of the Fermi level by changing the concentration of oxygen vacancies δ through oxidizing and reducing treatments. The energy band positions of LSC and LSF are studied by interface formation with different compounds, indicating that the identified charge transition levels are comparable to those in other perovskite-type materials.

II. EXPERIMENT

A. Sample preparation

All Sr-doped $LaCoO_3$ and $LaFeO_3$ thin film samples are prepared in the Darmstadt Integrated System for Materials Research (DAISY-MAT) [14]. The system combines multiple chambers for thin film deposition and surface treatments. $La_{0.6}Sr_{0.4}CoO_3$ and $La_{0.6}Sr_{0.4}FeO_3$ targets were purchased from Alineason (Frankfurt, Germany). SiO_2 (quartz) substrates from Alineason and c-cut Al_2O_3 (sapphire) substrates from CrysTec (Berlin, Germany) are used as substrates. All substrates have a dimension of $10 \times 10 \times 0.5\,mm^3$. All substrates are cleaned in an ultrasonic bath in acetone, ethanol, and isopropanol, each for 10 min. Platinum contacts were deposited on the edges of the substrates via DC sputtering to enable an electrical contact between sample, mask and the sample holder to avoid charging during XPS measurements.

LSC and LSF thin films are deposited by radio-frequency (RF) magnetron sputtering. The LSC thin films were deposited with a substrate temperature of 600° C, a gas pressure of 2 Pa (using an Ar/O_2 mixture with an O_2 content of 2%) and an applied RF-power of 25 W on a 2″ diameter target. The LSF thin films are deposited with a substrate temperature of 400° C, a gas pressure of 0.5 Pa (using an Ar/O_2 mixture with an O_2 content of 5%) and an applied RF-power of 25 W. The RuO_2 layers for interface studies are deposited at room temperature from a metallic Ru target in an Ar/O_2 gas mixture with an O_2 content of 7.5% with a pressure of 1 Pa and an applied DC power of 10 W.

B. Oxidative and reductive treatments

For the postsurface reduction treatment, the thin films are exposed to water pulses in an atomic layer deposition chamber which is connected to the system. Water pulses were released 30 times in a consecutive interval with an exposure time of 0.5 s and a rest period in between the pulses of about 60 s. During the water pulse, the ALD-3-valve to the water source opens and the pressure rises to about 2×10^{-4} mbar. Such treatments have repeatedly shown to have a strongly reducing effect on materials such as $BiVO_4$, $BiFeO_3$, NiO, and others [21,29,30]. Subsequent oxygen plasma treatments are performed at 200° C using a Tectra GenII plasma source (Frankfurt, Germany) in an atomic mode at an oxygen flow of 3 sccm at a pressure of 10^{-3} mbar. The power supply of the plasma source is set to 40 mA and the plasma is applied for 15 min.

C. X-ray photoelectron spectroscopy

A Physical Electronics 5700 Electron Spectrometer (Physical Electronics, Chanhassan, MN) is employed for the sample characterization by x-ray photoelectron spectroscopy with monochromatic Al Kα radiation with a photon energy of

1486.6 eV. The energy resolution determined from the Gaussian broadening of the Fermi edge of a clean silver (Ag) is 400 meV. The work function of the spectrometer is calibrated using a clean Ag standard sample by setting the Fermi edge of it to zero binding energy. The calibration is further refined by comparing the binding energy shift of the Ag $3d_{5/2}$ core level to the reference value of 368.26 eV [31].

D. Band alignment

The energy band alignments are investigated by interface experiments starting with a clean substrate [32–34]. A (001) oriented Nb-doped $SrTiO_3$ single crystal with dimension $5 \times 5 \times 0.5\,mm^3$ is used. Prior to stepwise deposition of LSC, the crystal is annealed at 400° C first in 0.5 Pa oxygen and subsequently for 2 hrs in a vacuum to remove hydrocarbon and hydroxide adsorbates. To determine the energy band position of LSF, RuO_2 is stepwise deposited onto a previously grown LSF thin film substrate. XP-core level spectra are recorded after each deposition step to monitor the interface formation process, continuing until the signal of the substrate is attenuated.

III. RESULTS AND DISCUSSION

A. Surface treatments

Photoelectron spectra of the O 1*s* and Sr 3*d* core levels and of the valence bands (VB) of as-deposited and treated LSC and LSF thin films are displayed in Fig. 2. The black, blue, and gray spectra represent the sample after deposition (As), after water exposure (H_2O) at 200° C for LSC, and 120° C for LSF and after oxygen plasma (O_2) treatment at 200° C, respectively.

In agreement with the literature, the line shape of the Sr 3*d* emission cannot be described by a single $3d_{5/2} - 3d_{3/2}$ spin-orbit doublet with a nominal branching ratio of 3:2 [13,40–42]. As the second doublet at higher binding energy is known to be enhanced under more surface sensitive measurement conditions, it is typically assigned to a SrO surface phase generated by partial segregation of the Sr acceptors. The segregation of acceptors is particularly expected under oxidizing conditions as the Gibbs formation energy of the Sr'_{La} acceptors increases with reducing Fermi level, and therefore, lowers its solubility [14]. We would like to mention here that the surface component of the Sr 3*d* emission is not necessarily related to a chemically different Sr phase. A surface component is also well known for the Ba 3*d* and Ba 4*d* emissions of a variety of materials, such as (Ba,Sr)TiO_3 (BST) [43]. In the case of BST, the intensity ratio of the surface to the bulk component increases substantially with decreasing Ba content, while the overall amount of Ba follows that of the composition of the bulk [44]. This, and several other observations exclude a BaO phase as origin of the Ba-related surface component of BST but rather points towards an (unresolved) electronic origin of the surface component. In the case of BST thin films it was demonstrated by Baniecki *et al*. that the Sr 3*d* emission also exhibits a (weaker) surface component [43].

The O 1*s* emission is dominated by a main peak around a binding energy of ≈529 eV, which is related to lattice oxygen. While the O 1*s* emission of the as-deposited and the water

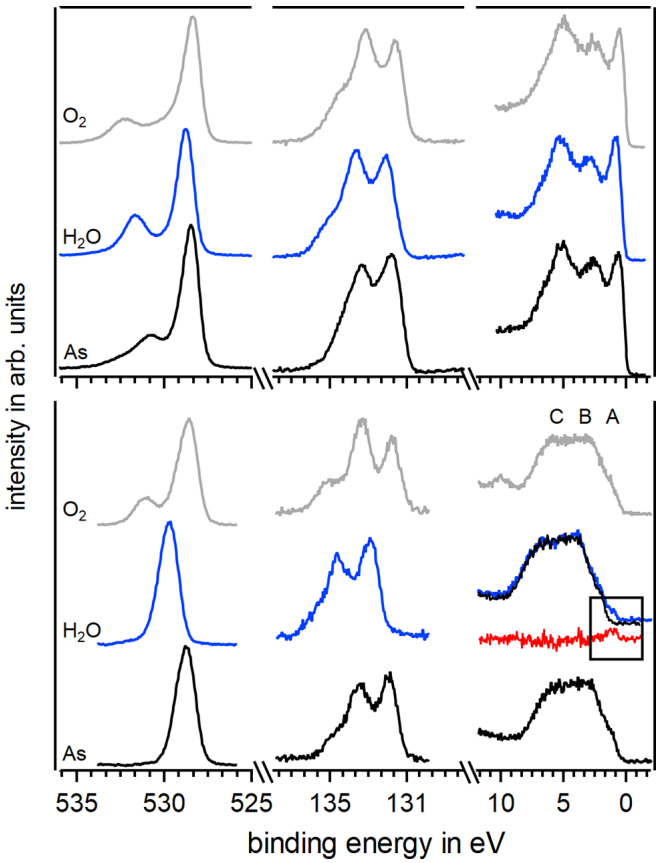


FIG. 2. X-ray photoelectron core level and valence band spectra (right column) of LSC (top) and LSF (bottom) thin film samples after deposition (As) in black, water exposure (H_2O) treatment in blue and oxygen plasma treatment (O_2) in gray. From the O 1*s* (left column), Sr $3d_{5/2}$ (middle column) core levels, the formation of SrO surface species are observed. Changes upon H_2O treatment, observed in the LSF VB spectra are indicated inside the box. The red line corresponds to the difference between the H_2O exposure and deposition. The labels A to C indicate common features reported for valence band spectra of LSF [35–39].

treated LSF is rather symmetric, additional high binding energy peaks are observed for LSC for every treatment. For LSF, an additional high binding energy emission is only observed after oxygen plasma treatment. The high binding energy O 1*s* features might be related to SrO, $Sr(OH)_2$ [13,45], or SrO_2, suggesting a relation to a Sr-related surface phase. However, Nenning *et al*. mentioned that the intensity of the high binding O 1*s* emission does not correlate with that of the Sr 3*d* surface component [13], indicating a different origin. This finding agrees with the current result, which does not reveal a high binding energy O 1*s* emission for as-deposited and water-treated LSF. The appearance of a high binding energy surface component in the Sr 3*d* core level for both LSC and LSF, but only for LSC in the O 1*s* core level might be explained if it is assumed that the surface component of the Sr 3*d* core level has an electronic origin as discussed above. With such a scenario for Sr 3*d*, the high binding energy O 1*s* peak cannot be assigned to a Sr-related surface phase. Alternatively, it might be related to oxidized oxygen species (O_O^-), which can be either lattice oxygen ions with trapped holes or oxygen

dimers adsorbed on the surface. The latter are to be expected for the oxygen plasma treated samples [46]. However, based on the presented results the origin of the high binding energy components in Sr 3*d* and O 1*s* core levels cannot be resolved. This does not affect the determination of the Fe and Co oxidation states and the Fermi levels in the materials, leaving the conclusions of this article unaffected.

The valence bands of LSF (LSC) are dominated by Fe 3*d* (Co 3*d*) and O 2*p* states [35,47]. The LSF valence band spectra depicted in Fig. 2 show three features (A to C), in agreement with spectra reported in the literature [35–39]. The three features are less pronounced and have different relative intensities as, for example, those reported by Wadati *et al.* [35]. However, other valence band spectra reported in the literature also reveal differently pronounced features (A to C) [36–39]. The valence band spectra presented in Fig. 2 fit well into the variation of spectra reported in literature, although the spectra reported in the literature are all recorded from epitaxial thin films, while the films used in this work are polycrystalline. To further confirm that the valence band spectra in Fig. 2 are representative for LSF, a comparison to valence band spectra recorded with the same setup from polycrystalline bulk ceramic pellets with the same Sr content is provided in the Supplemental Material [48]. The overall shape of the valence band of the LSF sample does not change substantially with the different treatments. Only an additional small emission appears above the VBM after water exposure, which is highlighted by a black square in Fig. 2. The additional emission after water exposure, which is attributed to reduced Fe^{2+} species [21,49–51] becomes evident after subtracting the VB spectra of the as-deposited sample, as indicated by the red curve. Additional evidence for an assignment of the small feature at the top of the valence band maximum is provided in the Supplemental Material [48], where Fe 2*p* and valence band spectra of a 2 % Fe-doped $BaTiO_3$ sample are reported. By different sample treatments, the oxidation state of Fe can be changed from Fe^{3+} to Fe^{2+}. The additional states above the valence band maximum are present only in the reduced state. The shape of the LSC valence band also exhibits no pronounced changes upon reduction or oxidation. It is noted, however, that the intensity of the leading valence band peak at ≈1 eV binding energy is higher after the reducing water treatment. The change of intensity of the leading valence band peak is further emphasized in the Supplemental Material [48], which includes spectra recorded from a 1 nm thick LSC film deposited onto Nb-doped $SrTiO_3$. For this sample, the oxidation state of Co could be changed reversibly from +3 to +2. The different changes in the valence bands upon lowering the oxidation state from +3 to +2 is possibly related to the different electronic configuration of the transition metals, which is changing from $d^5 \rightarrow d^6$ and from $d^6 \rightarrow d^7$ in the case of LSF and LSC, respectively.

B. Oxidation states of transition metals

As indicated by the valence band spectra, some Fe^{2+} (Co^{2+}) oxidation states are observed after the water treatments. This observation is confirmed by the Fe 2*p* and the Co 2*p* spectra, which are displayed in Fig. 3, in which the arrow and star indicate the formation of partially reduced Co^{2+} and Fe^{2+} after the water treatments, respectively. Apart from the binding energy shifts of the main features of the peaks, which are in parallel to the shifts of the Sr 3*d* and O 1*s* core levels in Fig. 3, small but notable changes in the peak shapes are observed after each treatment. For the as-deposited LSC sample, the binding energy of the Co $2p_{3/2}$ peak is located at a binding energy of 779.81 eV with a satellite peak appearing about 9.75 eV higher in energy. This energy difference between the Co $2p_{3/2}$ and its satellite peak is consistent with the Co^{3+} oxidation state [52–54]. After water exposure, the Co 2*p* satellite peak changes. In particular, the valley between the main peak and the satellite becomes filled, which is indicated by the arrow in Fig. 3. After the subsequent O_2 plasma treatment, the valley appears again. The binding energy difference between the Co $2p_{3/2}$ and the additional satellite peak filling the valley is ≈6 eV, aligning with literature values for

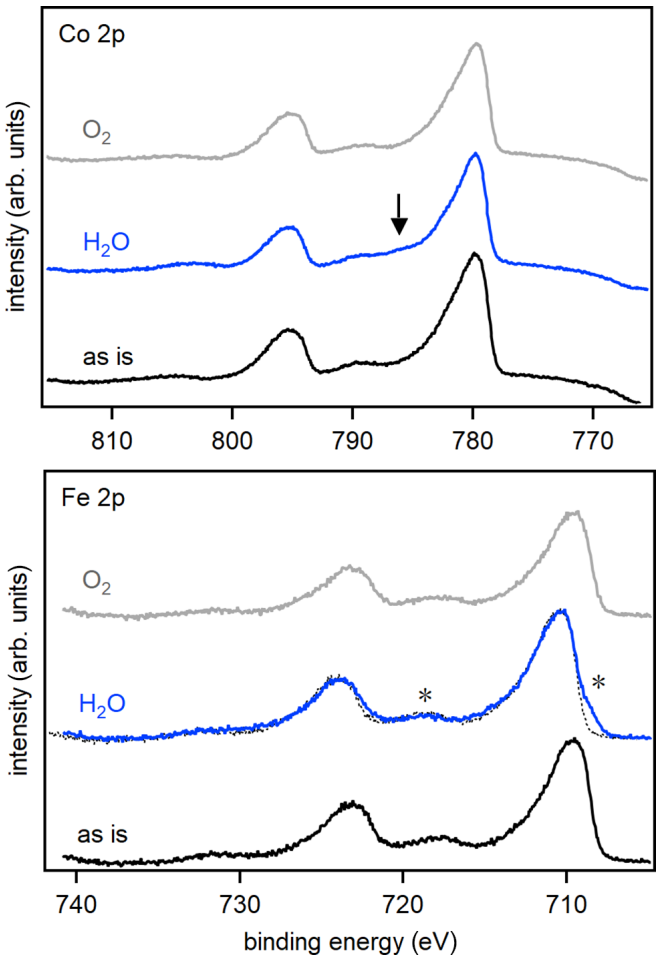


FIG. 3. X-ray photoelectron spectra of the Co 2*p* (top) and Fe 2*p* (bottom) core levels of LSC and LSF thin films recorded after deposition (As) in black, water exposure (H_2O) treatment in blue, and oxygen plasma treatment (O_2) in gray. The arrow and star indicate changes in the Co 2*p* and Fe 2*p* core levels upon water exposure. To better emphasize the partial reduction of Fe^{3+} to Fe^{2+} after water exposure, the spectrum (blue) is displayed on top of the as-deposited (black) sample, which contains only Fe^{3+}. In the Supplemental Material, additional spectral features of Fe^{2+} and Co^{2+} are provided as further supporting evidence [48].

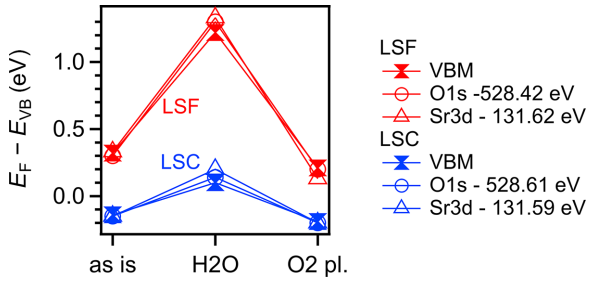


FIG. 4. Binding energies of O 1s, Sr 3$d_{5/2}$, and valence band maxima for LSC and LSF after deposition (as is), after water exposure (H_2O) and after oxygen plasma treatment (O_2 pl.). The uncertainty of the binding energies is ≈0.1 eV.

Co^{2+} [21,53,54]. The changes of the Co 2p emission with the oxidation state of Co are also emphasized by additional spectra in the Supplemental Material [48]. Hence, a mixture of Co^{2+} and Co^{3+} is present in the sample after water exposure and the corresponding Fermi level position (see below) will correspond to the $Co^{2+/3+}$ charge transition level.

The Fe 2$p_{3/2}$ peak of the as-deposited LSF sample exhibits a binding energy of ≈710.1 eV and a satellite peak at ≈7.8 eV higher binding energy, which are characteristic for Fe^{3+} [55]. After water exposure, a shoulder appears at the low binding energy side of both spin-orbit components of the Fe 2p emission (see star in Fig. 3 for the Fe 2$p_{3/2}$ component). The appearance of the shoulder is accompanied by a slight reduction of the satellite intensity. The changes clearly indicate the presence of Fe^{2+} species [13,21,56]. The partial reduction of $Fe^{3+/2+}$ is clearly observed in both valence band and Fe 2p core level spectra. Both features were observed and described in the literature for partially reduced Fe^{2+} compounds such as in Fe_2O_3 [20] and $BiFeO_3$ [21]. Additional Fe^{2+} and valence band spectra for Fe-doped $BaTiO_3$ are provided in the Supplemental Material [48]. As for LSC, a mixture of Fe^{2+} and Fe^{3+} is present in the sample after water exposure and the corresponding Fermi level position will correspond to the $Fe^{2+/3+}$ charge transition level.

C. Binding energy shifts and charge transition levels

The binding energies with respect to the Fermi level of the O 1s and the Sr 3$d_{5/2}$ core levels and of the valence band maxima are presented in Fig. 4. The valence band maxima are determined by the intersection of the linearly extrapolated edge of the valence band with the background emission. Core-level to valence band maximum binding energy differences, as indicated in the legend of Fig. 4, are subtracted from the core-level binding energies. This illustrates the parallel shift of all levels as should be the case if the shifts are caused only by changes of the Fermi level. Changes in the chemical state of the sample should result in different shifts. The parallel binding energy shifts of the O 1s and Sr 3$d_{5/2}$ core levels confirm that the second components in the core-level spectra do not influence the determination of the Fermi level. For the as-deposited and oxygen plasma treated LSC film, the Fermi level is below the valence band maximum as in degenerately doped p-type semiconductors, in good agreement with the literature [13]. In the case of the water-treated LSF film, the determination of the valence band maximum does not include the additional small feature, which is only present after water exposure and can be assigned to the presence of Fe^{2+}.

It is evident from Fig. 4 that the binding energies of the LSC emissions are consistently lower than than those of LSF. In agreement with previous experiments in which water exposure raised the Fermi level at different oxide surfaces [21,29,30], the binding energies of the O 1s and the Sr 3$d_{5/2}$ core levels and that of the valence band maximum (VBM) shift to higher energies after H_2O treatment. After the oxidative oxygen plasma treatments, the binding energies are reduced to values even lower than for the starting conditions, indicating a stronger oxidation of the samples. The overall difference in binding energy between the water-treated (highest binding energies) and the oxygen-plasma-treated (lowest binding energies) films amounts to 1.10 ± 0.1 eV for LSF and to 0.35 ± 0.05 eV for LSC. It is mentioned that the generally lower Fermi levels in LSC compare well with the higher electronic conductivity of LSC as compared to LSF [13,57].

As discussed above, the valence bands as well as the Fe 2p and Co 2p core-level spectra both indicate the presence of a mixture of 2+ and 3+ oxidation states of the transition metal cations after water treatment. The partial reduction to Fe^{2+} and Co^{2+} in LSF and LSC after water exposure results from an increase of the Fermi level, as induced by an increase of the oxygen vacancy concentration δ. According to charge neutrality (1), higher oxygen vacancy concentrations can be compensated by trapped electrons, i.e., by reduced cation species. In such a case, the oxygen vacancy concentration δ needs to exceed half of the Sr concentration. The reduced states of the samples are directly connected to a higher binding energy. As the water-treated samples contain a mixture of 2+ and 3+ states, it is possible to assign the Fermi level measured after water exposure to the 2 + /3+ charge transition within the thermal broadening of the Fermi distribution function (≈100 meV at room temperature). According to Fig. 4, the $Fe^{2+/3+}$ charge transition is determined at 1.25 ± 0.05 eV above the valence band maximum of LSF and the $Co^{2+/3+}$ charge transition at 0.15 ± 0.05 eV above the valence band maximum of LSC. This result compares well with the previous measurement on $Bi(Fe,Co)O_{3-\delta}$ in which the $Fe^{2+/3+}$ transition was found 0.85 eV higher in energy than the $Co^{2+/3+}$ transition. For a direct quantitative comparison of the charge transition levels, the alignment of the energy bands of LSF and LSC is required, which will be treated in the next section.

The exposure of the samples to an oxygen plasma constitutes a strongly oxidative treatment, which is also evident from the low Fermi levels observed for the oxygen-plasma-treated samples. Formally, an oxidation of LSF or LSC by reducing δ could be accompanied by an oxidation of Fe or Co to the 4+ oxidation state. However, neither the valence bands nor the Fe 2p and Co 2p spectra provide any evidence for an increase of the oxidation state beyond +3. This observation is consistent with the literature, in which no changes of the Fe 2p and Co 2p spectra are observed for cases where Fe^{4+} or Co^{4+} might be expected [13,58]. The absence of spectral evidence for the oxidation of Fe or Co might be explained by identical spectral signatures or by the fact that Fe and Co are not oxidized. As expressed by Eq. (1), a reduction of

the oxygen vacancy concentration can also be compensated for by the generation of free holes, or by the oxidation of oxygen. A lack of oxidation of Co in LSC is not surprising, as the $Co^{2+/3+}$ charge transition occurs just 150 meV above the valence band maximum. An oxidation to Co^{4+} would require Fermi level deep below the valence band maximum, hence a substantial removal of electrons from the valence band. The presence of a high concentration of holes and a Fermi level inside the valence band of LSC is consistent with the high electronic conductivity of the compound. However, some of the holes generated in the valence band might be localized on oxygen sites: $O^{2-} \rightarrow O^{-}$ [58,59]. The latter might be related to the high binding energy peak in the O 1*s* spectra.

Regarding the presence of Fe^{4+} in oxides, it was demonstrated for $BaFeO_3$ that an oxidation of oxygen is preferred against the oxidation of Fe [60]. However, in contrast to LSC, the Fermi level in LSF after oxygen plasma treatment is still clearly above the valence band maximum. It may also be that the oxygen plasma treatment does not remove enough oxygen vacancies to generate Fe^{4+}. On the other hand, oxidation of LSF as compared to undoped $LaFeO_3$ is indicated by the appearance of the so-called *split-off hole state*, which can be observed, in optical absorption or x-ray absorption studies [35,39].

D. Alignment of charge transition levels

To compare the $Co^{2+/3+}$ and $Fe^{2+/3+}$ charge transition levels with each other and with other perovskite-type materials, the energetic positions of the valence band maxima of LSC and LSF relative to each other and to the valence band maxima of other materials has to be determined. Such an alignment can be obtained by different means, involving, for example, an alignment of the vacuum level or of flat band potentials determined from electrochemical impedance spectroscopy at solid/liquid interfaces [28]. In the present context, an alignment provided from direct measurements of solid/solid interfaces is expected to be the best reference for a comparison of charge transition levels in solids. Such an alignment can be obtained, for example, by studying interface formation with XPS through the stepwise deposition of ultrathin films onto clean substrate surfaces [32–34].

As demonstrated above, (La, Sr)$CoO_{3-\delta}$ has a Fermi level inside the valence band and the Fermi level exhibits only a small variation. Due to the pinning of the Fermi level in LSC, a contact partner which exhibits no Fermi level pinning is required to avoid modification of the band alignment [61]. $SrTiO_3$ is commonly used as substrate in such experiments and its interface behavior is well studied [62–70]. The XP spectra and the extraction of the energy band alignment are provided in the Supplemental Material [48]. The resulting alignment with the valence band maximum of LSC being 2.15 ± 0.1 eV above that of $SrTiO_3$ is depicted on the left side of Fig. 5.

The alignment of the energy bands of (La, Sr)$FeO_{3-\delta}$ is derived by stepwise deposition of RuO_2 onto a (La, Sr)$FeO_{3-\delta}$ substrate prepared in the same vacuum system as a first step of the experiment. The evolution of the XP spectra with increasing film thickness and the extraction of the band alignment are described in the Supplemental Material [48]. The alignment with $SrTiO_3$ is then obtained by combining the result with measurements of the $SrTiO_3/RuO_2$ interface, which has been reported previously [70]. As illustrated in Fig. 5, the valence band maximum of (La, Sr)$CoO_{3-\delta}$ is eventually found to be 0.45 eV higher in energy than that of (La, Sr)$FeO_{3-\delta}$ assuming transitivity of the band alignments [71]. Additional interface experiments carried out with $BaTiO_3$ as a reference material reveal an identical alignment between LSC and LSF, confirming the transitivity of the derived alignment. The higher valence band maximum of LSC compared to that of LSF is likely be assigned to a different hybridisation of the 3*d* orbitals of Co and Fe with the O 2*p* orbitals.

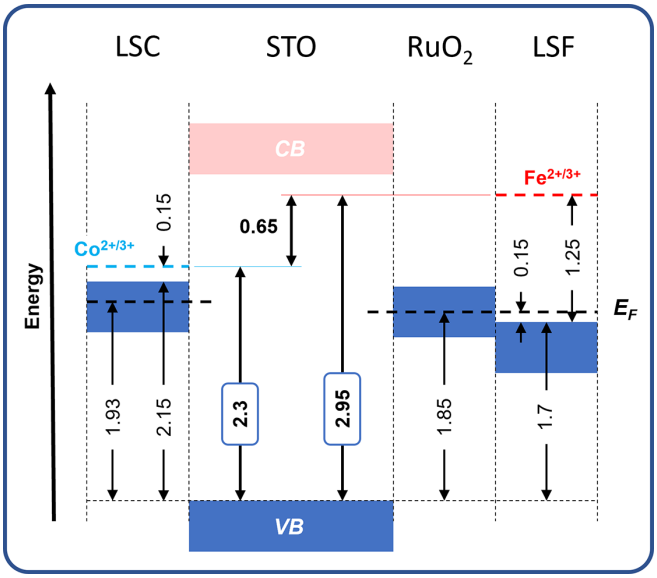


FIG. 5. Energetic alignment of the $Co^{2+/3+}$ and the $Fe^{2+/3+}$ charge transition levels in (La, Sr)$CoO_{3-\delta}$ and (La, Sr)$FeO_{3-\delta}$, respectively. The alignment is performed via aligning the energy bands with those of $SrTiO_3$ by means of XPS interface experiments. The $Co^{2+/3+}$ charge transition level is 0.65 eV lower in energy than the $Fe^{2+/3+}$ charge transition level. The energy band alignments at the $SrTiO_3$/LSCO and the LSFO/RuO_2 are extracted from experiments presented in the Supplemental Material [48] and that at the $SrTiO_3/RuO_2$ interface from [70]. All numbers are given in electronvolts. For simplicity, band gap values are neglected.

With the determined energy band alignment between LSC and LSF, the $Co^{2+/3+}$ charge transition is eventually found to occur 0.65 eV lower in energy than the $Fe^{2+/3+}$ charge transition. This difference compares well with the charge transition levels of Co and Fe in Bi(Fe,Co)$O_{3-\delta}$, where the $Co^{2+/3+}$ transition is 0.85 eV lower than the $Fe^{2+/3+}$ transition [21]. The slightly larger difference between the $Co^{2+/3+}$ and the $Fe^{2+/3+}$ CTL in Bi(Fe,Co)$O_{3-\delta}$ may be related to the contribution of Bi 6*s* orbitals to the electronic states near the valence band maximum [72,73].

E. Relation to (La,Sr)(Co,Fe)$O_{3-\delta}$

The results above are closely related to the performance of a widely used mixed ionic-electronic conductors: (La,Sr)(Co,Fe)$O_{3-\delta}$ (LSCF). In pure LSC, the acceptor doping results in a Fermi level below the E_{VB} and charge

compensation of the Sr'_{La} acceptors will be mostly electronic by holes in the valence band. Therefore, the oxygen vacancy concentration and oxygen ion conductivity is limited. On the other hand, the Fermi level will not reach the valence band maximum in pure LSF. Hence, the concentration of holes and thereby electronic conduction will be limited. Adding Co to LSF will have two effects: (i) as part of the Co may remain in the 2+ oxidation state, it will act as an additional acceptor and thereby increase either the hole or the oxygen vacancy concentration; (ii) as the valence band maximum will be shifted upwards, induced by new Co states near the Fermi level, the concentration of holes will be increased even if the Fermi level is not changing. Analogously, the addition of Fe to LSC will lower the E_{VB} and thereby decrease the hole and increase the oxygen vacancy concentration. These arguments explain the superior behavior of LSCF as mixed-ionic-electronic conductor as compared to pure LSC and LSF.

IV. SUMMARY AND CONCLUSION

$La_{0.6}Sr_{0.4}CoO_3$ and $La_{0.6}Sr_{0.4}FeO_3$ thin films have been prepared by radio frequency magnetron sputtering. XPS measurements were performed, as this technique uniquely allows simultaneous probing of the Fermi level and oxidation states. The variation of the Fermi level between most reducing (water exposure) and most oxidizing (oxygen plasma) treatments amounts to 1.10 ± 0.1 eV for LSF and to 0.35 ± 0.05 eV for LSC. In all cases, the Fermi levels with respect to the valence band maximum of LSC are lower than those of LSF. While the Fermi level is always inside the energy gap in the case of LSF, the Fermi level falls below the valence band maximum of LSC under more oxidizing conditions. The lower Fermi level in LSC correspond well with the higher electronic conductivity of LSC as compared to LSF.

Both Co and Fe exhibit an oxidation state of +3 for lower values of the Fermi level. Even after oxygen plasma treatment, the Co $2p$ and Fe $2p$ spectra provide no evidence for a higher oxidation state than +3. There is no doubt that the potential presence of Fe^{4+} and Co^{4+} in LSF and LSC is of fundamental importance and has higher relevance than that of the reduced 2+ species. However, it is not yet possible to conclude about the presence of Fe^{4+} or Co^{4+}, so the $Fe^{3+/4+}$ and $Co^{3+/4+}$ charge transition levels cannot be determined but only the $(Co/Fe)^{2+/3+}$ transitions are accessible. Under reducing conditions (water exposure), Co and Fe are present in a mixture of 2+ and 3+ oxidation states. In this case, the Fermi level corresponds to the 2 + /3+ charge transition, which is determined to be 0.15 eV and 1.25 eV above the valence band maxima of LSC and LSF, respectively.

XPS interface analysis is performed to align the valence band maxima of LSC and LSF relative to those of $SrTiO_3$, revealing a valence band maximum energy of LSC being 0.45 eV higher than that of LSF. This reduces the difference between the $Co^{2+/3+}$ and the $Fe^{2+/3+}$ charge transition levels on the same energy scale to 0.65 eV, in reasonable agreement with the 0.85 eV difference in $Bi(Fe,Co)O_{3-\delta}$.

The present contribution demonstrates how charge transition levels of species can be quantified by means of x-ray photoelectron spectroscopy with *in situ* manipulation of the Fermi level by oxidizing and reducing sample treatments and how these charge transition levels can be aligned on a general energy scale by means of XPS interface analysis. This highlights the unique feature of XPS as the only experimental technique being able to simultaneously detect the Fermi level of a material and the chemical states of its constituents.

The close agreement of the difference between the $Co^{2+/3+}$ and the $Fe^{2+/3+}$ charge transition levels in LSC(F) with those in $Bi(Fe,Co)O_{3-\delta}$ indicates that the charge transition levels are, at least partially, transferable from one material to another as also suggested for classical semiconductor compounds [22–24]. A transferability of CTLs would constitute a substantial benefit for the selection of dopants to adjust material properties as the effect of different dopants would become predictable.

ACKNOWLEDGMENTS

The presented work was supported by the Deutsche Forschungsgemeinschaft (DFG) within the collaborative research center FLAIR (Fermi level engineering applied to oxide electroceramics, Grant No. 463184206–SFB 1548). NAP-XPS beamtime for the Fe-doped $BaTiO_3$ included in the Supplemental Material was granted at the ISISS endstation of BESSY II at Helmholtz-Zentrum Berlin, ISISS beamline, operated by Fritz-Haber-Institute. Assistance of Ali Hebatallah and Raoul Blume during beamtime is gratefully acknowledged.

DATA AVAILABILITY

The data that support the findings of this article are openly available [74].

[1] J. B. Goodenough, Electronic and ionic transport properties and other physical aspects of perovskites, Rep. Prog. Phys. **67**, 1915 (2004).

[2] *Mixed Conducting Ceramic Membranes* edited by X. Zhu and W. Yang (Springer, Berlin, 2017).

[3] J. A. Kilner and M. Burriel, Materials for intermediate-temperature solid-oxide fuel cells, Annu. Rev. Mater. Res. **44**, 365 (2014).

[4] H. Wang, K. H. L. Zhang, J. P. Hofmann, V. A. de La Peña O'Shea, and F. E. Oropeza, The electronic structure of transition metal oxides for oxygen evolution reaction, J. Mater. Chem. A **9**, 19465 (2021).

[5] T. Arima, Y. Tokura, and J. B. Torrance, Variation of optical gaps in perovskite-type 3d transition-metal oxides, Phys. Rev. B **48**, 17006 (1993).

[6] M. D. Scafetta, Y. J. Xie, M. Torres, J. E. Spanier, and S. J. May, Optical absorption in epitaxial $La_{1-x}Sr_xFeO_3$ thin films, Appl. Phys. Lett. **102**, 081904 (2013).

[7] A. Chainani, M. Mathew, and D. D. Sarma, Electron-spectroscopy study of the semiconductor-metal transition in $La_{1-x}Sr_xCoO_3$, Phys. Rev. B **46**, 9976 (1992).

[8] C.-L. Ma and J. Cang, First principles investigation on the band gap of the ground state of $LaCoO_3$, Solid State Commun. **150**, 1983 (2010).

[9] I. A. Abdel-Latif, A. F. Hegab, A. A. Azab, and Kh M. Roumaih, Study on crystal structure, electrical and magnetic properties of $LaFe_xCo_{1-x}O_3$ prepared by sol-gel method, J. Solid State Chem. **325**, 124144 (2023).

[10] A. Petrov, Crystal structure, electrical and magnetic properties of $La_{1-x}Sr_xCoO_{3-y}$, Solid State Ionics **80**, 189 (1995).

[11] E. Bucher and W. Sitte, Defect chemical analysis of the electronic conductivity of strontium-substituted lanthanum ferrite, Solid State Ionics **173**, 23 (2004).

[12] W.-W. Zhang, E. Povoden-Karadeniz, Y. Shang, P. V. Hendriksen, and M. Chen, Phase equilibria and defect chemistry of the La-Sr-Co-O system, J. Eur. Ceram. Soc. **43**, 4419 (2023).

[13] A. Nenning, A. K. Opitz, C. Rameshan, R. Rameshan, R. Blume, M. Hävecker, A. Knop-Gericke, G. Rupprechter, B. Klötzer, and J. Fleig, Ambient pressure XPS study of mixed conducting perovskite-type SOFC cathode and anode materials under well-defined electrochemical polarization, J. Phys. Chem. C **120**, 1461 (2016).

[14] A. Klein, K. Albe, N. Bein, O. Clemens, K. A. Creutz, P. Erhart, M. Frericks, E. Ghorbani, J. P. Hofmann, B. Huang, B. Kaiser, U. Kolb, J. Koruza, C. Kübel, K. N. S. Lohaus, J. Rödel, J. Rohrer, W. Rheinheimer, R. A. de Souza, and V. Streibel *et al.*, The Fermi energy as common parameter to describe charge compensation mechanisms: A path to Fermi level engineering of oxide electroceramics, J. Electroceram. **51**, 147 (2023).

[15] S. Anand, M. Y. Toriyama, C. Wolverton, S. M. Haile, and G. J. Snyder, A convergent understanding of charged defects, Acc. Mater. Res. **3**, 685 (2022).

[16] A. Klein and D. Sudarikov, The physics of defect chemistry and the chemistry of defect physics, Phys. Chem. Chem. Phys. **27**, 6390 (2025).

[17] C. Freysoldt, B. Grabowski, T. Hickel, J. Neugebauer, G. Kresse, A. Janotti, and C. G. Van de Walle, First-principles calculations for point defects in solids, Rev. Mod. Phys. **86**, 253 (2014).

[18] A. Klein, Transparent conducting oxides: Electronic structure–property relationship from photoelectron spectroscopy with in-situ sample preparation, J. Am. Ceram. Soc. **96**, 331 (2013).

[19] A. Klein, Interface properties of dielectric oxides, J. Am. Ceram. Soc. **99**, 369 (2016).

[20] C. Lohaus, A. Klein, and W. Jaegermann, Limitation of Fermi level shifts by polaron defect states in hematite photoelectrodes, Nat. Commun. **9**, 4309 (2018).

[21] N. S. Bein, P. Machado, M. Coll, M. Chen, M. Makarovic, T. Rojac, and A. Klein, Electrochemical reduction of undoped and cobalt-doped $BiFeO_3$ induced by water exposure: Quantitative determination of reduction potentials and defect energy levels using photoelectron spectroscopy, J. Phys. Chem. Lett. **10**, 7071 (2019).

[22] A. Zunger, Theory of 3d transition atom impurities in semiconductors, Annu. Rev. Mater. Sci. **15**, 411 (1985).

[23] J. M. Langer and H. Heinrich, Deep-level impurities: A possible guide to prediction of band-edge discontinuities in semiconductor heterojunctions, Phys. Rev. Lett. **55**, 1414 (1985).

[24] J. M. Langer, C. Delerue, M. Lannoo, and H. Heinrich, Transition-metal impurities in semiconductors and heterojunction band lineups, Phys. Rev. B **38**, 7723 (1988).

[25] C. G. van de Walle and J. Neugebauer, Universal alignment of hydrogen levels in semiconductors, insulators and solutions, Nature (London) **423**, 626 (2003).

[26] C. Linderälv, A. Lindman, and P. Erhart, A unifying perspective on oxygen vacancies in wide band gap oxides, J. Phys. Chem. Lett. **9**, 222 (2018).

[27] S. Chen and L.-W. Wang, Thermodynamic oxidation and reduction potentials of photocatalytic semiconductors in aqueous solution, Chem. Mater. **24**, 3659 (2012).

[28] A. Klein, Application of photoelectron spectroscopy to align the energy levels of photocatalysts, in *Applications of X-ray Photoelectron Spectroscopy to Catalytic Studies*, edited by S. Zafeiratos (World Scientific, Singapore, 2023), pp. 193–230.

[29] Y. Hermans, S. Murcia-López, A. Klein, and W. Jaegermann, $BiVO_4$ surface reduction upon water exposure, ACS Energy Lett. **4**, 2522 (2019).

[30] R. Poulain, J. Rohrer, Y. Hermans, C. Dietz, J. Brötz, J. Proost, M. Chatenet, and A. Klein, Origin of surface reduction upon water adsorption on oriented nio thin films and its relation to electrochemical activity, J. Phys. Chem. C **126**, 1303 (2022).

[31] *Handbook of X-Ray Photoelectron Spectroscopy: A Reference Book of Standard Spectra for Identification and Interpretation of XPS Data*, [reprint of the 1992 version] edited by J. Chastain and J. F. Moulder (Physical Electronics, Eden Prairie, MN, 1995).

[32] E. A. Kraut, R. W. Grant, J. R. Waldrop, and S. P. Kowalczyk, Precise determination of the valence-band edge in x-ray photoemission spectra: Application to measurement of semiconductor interface potentials, Phys. Rev. Lett. **44**, 1620 (1980).

[33] J. R. Waldrop, R. W. Grant, S. P. Kowalczyk, and E. A. Kraut, Measurement of semiconductor heterojunction band discontinuities by X-ray photoemission spectroscopy, J. Vac. Sci. Technol. A **3**, 835 (1985).

[34] A. Klein, Energy band alignment at interfaces of semiconducting oxides: A review of experimental determination using photoelectron spectroscopy and comparison with theoretical predictions by the electron affinity rule, charge neutrality levels, and the common anion rule, Thin Solid Films **520**, 3721 (2012).

[35] H. Wadati, D. Kobayashi, H. Kumigashira, K. Okazaki, T. Mizokawa, A. Fujimori, K. Horiba, M. Oshima, N. Hamada, M. Lippmaa, M. Kawasaki, and H. Koinuma, Hole-doping-induced changes in the electronic structure of $La_{1-x}Sr_xFeO_3$: Soft x-ray photoemission and absorption study of epitaxial thin films, Phys. Rev. B **71**, 035108 (2005).

[36] Z. Shen, Y. Zhuang, W. Li, X. Huang, F. E. Oropeza, E. J. M. Hensen, J. P. Hofmann, M. Cui, A. Tadich, D.-C. Qi, J. Cheng, J. Li, and K. H. L. Zhang, Increased activity in the oxygen evolution reaction by Fe^{4+}-induced hole states in perovskite $La_{1-x}Sr_xFeO_3$, J. Mater. Chem. A **8**, 4407 (2020).

[37] K. A. Stoerzinger, R. Comes, S. R. Spurgeon, S. Thevuthasan, K. Ihm, E. J. Crumlin, and S. A. Chambers, Influence of $LaFeO_3$ surface termination on water reactivity, J. Phys. Chem. Lett. **8**, 1038 (2017).

[38] C. Tian, C. Maheu, X. Huang, F. E. Oropeza, M. Major, J. Brötz, M. Einert, W. Donner, K. H. Zhang, and J. P. Hofmann, Evaluating the electronic structure and stability of epitaxially grown Sr-doped $LaFeO_3$ perovskite alkaline O_2 evolution model electrocatalysts, RSC Appl. Interfaces **2**, 122 (2025).

[39] L. Wang, Y. Du, P. V. Sushko, M. E. Bowden, K. A. Stoerzinger, S. M. Heald, M. D. Scafetta, T. C. Kaspar, and S. A. Chambers, Hole-induced electronic and optical transitions in

$La_{1-x}Sr_xFeO_3$ epitaxial thin films, Phys. Rev. Mater. **3**, 025401 (2019).

[40] E. J. Crumlin, E. Mutoro, Z. Liu, M. E. Grass, M. D. Biegalski, Y.-L. Lee, D. Morgan, H. M. Christen, H. Bluhm, and Y. Shao-Horn, Surface strontium enrichment on highly active perovskites for oxygen electrocatalysis in solid oxide fuel cells, Energy Environ. Sci. **5**, 6081 (2012).

[41] Z. Cai, M. Kubicek, J. Fleig, and B. Yildiz, Chemical heterogeneities on $La_{0.6}Sr_{0.4}CoO_{3-\delta}$ thin films–correlations to cathode surface activity and stability, Chem. Mater. **24**, 1116 (2012).

[42] A. K. Opitz, C. Rameshan, M. Kubicek, G. M. Rupp, A. Nenning, T. Götsch, R. Blume, M. Hävecker, A. Knop-Gericke, G. Rupprechter, B. Klötzer, and J. Fleig, The chemical evolution of the $La_{0.6}Sr_{0.4}CoO_{3-\delta}$ surface under SOFC operating conditions and its implications for electrochemical oxygen exchange activity, Top. Catal **61**, 2129 (2018).

[43] J. D. Baniecki, M. Ishii, T. Shioga, K. Kurihara, and S. Miyahara, Surface core-level shifts of strontium observed in photoemission of barium strontium titanate thin films, Appl. Phys. Lett. **89**, 162908 (2006).

[44] R. Schafranek, Kathodenzerstäubte (Ba,Sr)TiO_3-Dünnschichten für steuerbare Mikrowellenkomponenten: Material-, Bauteil- und Grenzflächeneigenschaften; https://tuprints.ulb.tu-darmstadt.de/id/eprint/1873, Ph.D. thesis, Technical University of Darmstadt, 2009.

[45] P. A. W. van der Heide, Systematic x–ray photoelectron spectroscopic study of $La_{1-x}Sr_x$–based perovskite–type oxides, Surf. Interface Anal. **33**, 414 (2002).

[46] S. Kashiwaya, J. Morasch, V. Streibel, T. Toupance, W. Jaegermann, and A. Klein, The work function of TiO_2, Surfaces **1**, 73 (2018).

[47] M. Abbate, J. C. Fuggle, A. Fujimori, L. H. Tjeng, C. T. Chen, R. Potze, G. A. Sawatzky, H. Eisaki, and S. Uchida, Electronic structure and spin-state transition of $LaCoO_3$, Phys. Rev. B **47**, 16124 (1993).

[48] See Supplemental Material at http://link.aps.org/supplemental/10.1103/tn7z-thjk for XP survey spectra recorded after different surface treatments, a comparison of the valence band spectra of LSF thin films and bulk ceramics, Fe2p and valence band spectra of 2% Fe-doped $BaTiO_3$ bulk ceramics revelaing changes of Fe oxidation state, Co2p and valence band spectra of LSC thin films on Nb-$SrTiO_3$ revealing changes of Co oxidation state, XP core level and valence band spectra recorded in the course of interface formation for determination of the energy band alignment at the $SrTiO_3$/LSC interface, as well as the XP core level and valence band spectra recorded in the course of the deposition of RuO_2 onto LSF for the determination of band alignment. The Supplemental Material contains Refs. [35–39,75].

[49] T. Fujii, F. M. F. de Groot, G. A. Sawatzky, F. C. Voogt, T. Hibma, and K. Okada, In situ XPS analysis of various iron oxide films grown by NO_2-assisted molecular-beam epitaxy, Phys. Rev. B **59**, 3195 (1999).

[50] C.R Brundle, T.J Chuang, and K. Wandelt, Core and valence level photoemission studies of iron oxide surfaces and the oxidation of iron, Surf. Sci. **68**, 459 (1977).

[51] R. J. Lad and V. E. Henrich, Photoemission study of the valence-band electronic structure in Fe_xO, Fe_3O_4, and α-Fe_2O_3 single crystals, Phys. Rev. B **39**, 13478 (1989).

[52] Z. Zhu, Y. Shi, C. Aruta, and N. Yang, Improving electronic conductivity and oxygen reduction activity in Sr-doped lanthanum cobaltite thin films: Cobalt valence state and electronic band structure effects, ACS Appl. Energy Mater. **1**, 5308 (2018).

[53] D. Ensling, A. Thißen, Y. Gassenbauer, A. Klein, and W. Jaegermann, In–situ preparation and analysis of functional oxides, Adv. Eng. Mater. **7**, 945 (2005).

[54] C. Lohaus, J. Morasch, J. Brötz, A. Klein, and W. Jaegermann, Investigations on RF-magnetron sputtered Co_3O_4 thin films regarding the solar energy conversion properties, J. Phys. D: Appl. Phys. **49**, 155306 (2016).

[55] L. A. Isupova and I. P. Prosvirin, X-ray photoelectron spectroscopy investigation of perovskites $La_{1-x}Sr_xFeO_{3-y}$ ($0 \leqslant x < 1.0$), prepared via a mechanochemical route, Russ. Chem. Bull. **62**, 1564 (2013).

[56] R. P. Gupta and S. K. Sen, Calculation of multiplet structure of core p -vacancy levels. II, Phys. Rev. B **12**, 15 (1975).

[57] J. Richter, P. Holtappels, T. Graule, T. Nakamura, and L. J. Gauckler, Materials design for perovskite SOFC cathodes, Monatsh. Chem. **140**, 985 (2009).

[58] M. Abbate, F. M. F. de Groot, J. C. Fuggle, A. Fujimori, O. Strebel, F. Lopez, M. Domke, G. Kaindl, G. A. Sawatzky, M. Takano, Y. Takeda, H. Eisaki, and S. Uchida, Controlled-valence properties of $La_{1-x}Sr_xFeO_3$ and $La_{1-x}Sr_xMnO_3$ studied by soft-x-ray absorption spectroscopy, Phys. Rev. B **46**, 4511 (1992).

[59] D. N. Mueller, M. L. Machala, H. Bluhm, and W. C. Chueh, Redox activity of surface oxygen anions in oxygen-deficient perovskite oxides during electrochemical reactions, Nat. Commun. **6**, 6097 (2015).

[60] M. F. Hoedl, C. Ertural, R. Merkle, R. Dronskowski, and J. Maier, The orbital nature of electron holes in $BaFeO_3$ and implications for defect chemistry, J. Phys. Chem. C **126**, 12809 (2022).

[61] S. Siol, J. C. Hellmann, S. D. Tilley, M. Graetzel, J. Morasch, J. Deuermeier, W. Jaegermann, and A. Klein, Band alignment engineering at Cu_2O/ZnO heterointerfaces, ACS Appl. Mater. Interfaces **8**, 21824 (2016).

[62] S. A. Chambers, T. Droubay, T. C. Kaspar, M. Gutowski, and M. van Schilfgaarde, Accurate valence band maximum determination for $SrTiO_3$(001), Surf. Sci. **554**, 81 (2004).

[63] R. Schafranek, S. Payan, M. Maglione, and A. Klein, Barrier heights at (Ba,Sr)TiO_3/Pt interfaces studied by photoemission, Phys. Rev. B **77**, 195310 (2008).

[64] S. A. Chambers, T. Ohsawa, C. M. Wang, I. Lyubinetsky, and J. E. Jaffe, Band offsets at the epitaxial anatase TiO_2/n-$SrTiO_3$(001) interface, Surf. Sci. **603**, 771 (2009).

[65] R. Schafranek, S. Li, F. Chen, W. Wu, and A. Klein, $PbTiO_3$/$SrTiO_3$ interface: Energy band alignment and its relation to the limits of Fermi level variation, Phys. Rev. B **84**, 045317 (2011).

[66] R. Schafranek, J. D. Baniecki, M. Ishii, Y. Kotaka, and K. Kurihara, The $SrTiO_3$/$BiFeO_3$ (001) interface: Commutativity of energy band discontinuities, New J. Phys. **15**, 053014 (2013).

[67] S. Balaz, Z. Zeng, and L. J. Brillson, Heterojunction band offsets and dipole formation at $BaTiO_3$/$SrTiO_3$ interfaces, J. Appl. Phys. **114**, 183701 (2013).

[68] T. Yajima, Y. Hikita, M. Minohara, C. Bell, J. A. Mundy, L. F. Kourkoutis, D. A. Muller, H. Kumigashira, M. Oshima, and

H. Y. Hwang, Controlling band alignments by artificial interface dipoles at perovskite heterointerfaces, Nat. Commun. **6**, 6759 (2015).

[69] S. A. Chambers, T. C. Kaspar, A. Prakash, G. Haugstad, and B. Jalan, Band alignment at epitaxial $BaSnO_3/SrTiO_3$(001) and $BaSnO_3/LaAlO_3$(001) heterojunctions, Appl. Phys. Lett. **108**, 152104 (2016).

[70] R. Giesecke, R. Hertwig, T. Bayer, C. A. Randall, and A. Klein, Modification of the schottky barrier height at the RuO_2 cathode during resistance degradation of Fe-doped $SrTiO_3$, J. Am. Ceram. Soc. **100**, 4590 (2017).

[71] S. Li, F. Chen, R. Schafranek, T. J. M. Bayer, K. Rachut, A. Fuchs, S. Siol, M. Weidner, M. Hohmann, V. Pfeifer, J. Morasch, C. Ghinea, E. Arveux, R. Günzler, J. Gassmann, C. Körber, Y. Gassenbauer, F. Säuberlich, G. Venkata Rao, and S. Payan *et al.*, Intrinsic energy band alignment of functional oxides, Phys. Status Solidi RRL **8**, 571 (2014).

[72] S. Li, J. Morasch, A. Klein, C. Chirila, L. Pintilie, L. Jia, K. Ellmer, M. Naderer, K. Reichmann, M. Gröting, and K. Albe, Influence of orbital contributions to the valence band alignment of Bi_2O_3, Fe_2O_3, $BiFeO_3$, and $Bi_{0.5}Na_{0.5}TiO_3$, Phys. Rev. B **88**, 045428 (2013).

[73] A. Walsh, D. J. Payne, R. G. Egdell, and G. W. Watson, Stereochemistry of post-transition metal oxides: Revision of the classical lone pair model, Chem. Soc. Rev. **40**, 4455 (2011).

[74] https://tudatalib.ulb.tu-darmstadt.de/handle/tudatalib/4685.

[75] A. Klein, T. Mayer, A. Thissen, and W. Jaegermann, Photoelectron spectroscopy in materials science and physical chemistry: Analysis of composition, chemical bonding and electronic structure of surfaces and interfaces, in *Methods in Physical Chemistry* Vol. 2, edited by R. Schäfer and P. C. Schmidt (Wiley-VCH, Weinheim, 2012).